Short-Range Millimeter-Wave Radar Perception in a Polar Environment

Alex Foessel, Sachin Chheda and Dimitrios Apostolopoulos
Robotics Institute, Carnegie Mellon University
Pittsburgh, PA 15213-3890
{afoessel, chheda, da1v}@ri.cmu.edu

***Abstract*–Autonomous vehicle operations in Antarctica challenge robotic perception. Flying ice and snow, changing illumination due to low sun angles and lack of contrast degrade stereo and laser sensing. Millimeter-wave radar offers remarkable advantages as a robotic perception modality because it is not as sensitive to the aforementioned conditions. Experiments with millimeter-wave radar in an Antarctic environment show minimal degradation of millimeter-wave sensing capabilities under blowing-snow conditions, as well as backscatter obtained from polar-terrain surfaces at grazing angles and detection of obstacles commonly found in polar areas. This paper presents issues relevant to short-range radar perception for a mobile robot in an Antarctic environment. The article describes the experiments and data-analysis procedures, and draws conclusions on the utility of millimeter-wave radar as a robotic sensor for obstacle avoidance and navigation in polar settings.**

***Keywords*–Millimeter-wave radar, millimeter-wave imaging, radar scattering, mobile robots, robot sensing.**

I. Introduction

Autonomous vehicle operations in Antarctica pose a challenge to robotic perception. Flying ice and snow, changing light conditions and lack of contrast compromise stereo and laser sensors aboard mobile robots. Millimeter-wave radar offers remarkable advantages as a mobile-robot sensor because it is not as sensitive to the aforementioned conditions. Obstacle avoidance and navigation can succeed under compromised visibility through the use of range data acquired by a scanning millimeter-wave radar.

Short-range radar-sensing issues motivated an experimental agenda with three facets. The first part of the study addresses perception of terrain and obstacles through blowing snow and ice, with the intention of estimating sensing noise introduced by the weather phenomena. The second part deals with the necessary conditions for backscatter at grazing from common types of polar terrain: blue ice, and soft and hard snow. The emphasis here is on the range of angles that enable polar-surface perception with millimeter waves. The third segment focuses on millimeter-wave short-range sensing and relates the footprint size at grazing angles with the beam model predictions.

In November 1998, a short-range millimeter-wave scanning radar was deployed at Patriot Hills, West Antarctica. Field experiments demonstrated that millimeter-wave radar has the potential to provide reliable sensing for a mobile robot. Ice and snow surface perception is feasible because of millimeter-wave terrain backscatter at grazing angles. Obstacle detection occurs under all visibility conditions. Sensing noise increases slightly in blowing snow, but no sensing impairment due to weather conditions was detected.

This paper presents related research and issues pertaining to the use of millimeter-wave radar for short-range sensing, field deployment and experiment description. The article also presents data analysis and conclusions on the utility of millimeter-wave radar as a robotic sensor for obstacle avoidance and navigation in polar settings.

A. Robotic Perception in a Polar Environment

Antarctic weather presents clear-sky days and cloudy days that obscure contrast as well as days with white-out condition with null surface visibility due to blowing snow and ice. Antarctic-terrain surfaces consist of blue-ice fields and areas with soft and hard snow. The blue-ice fields and snow-covered areas contain obstacles such as snow pits and mounds as well as rocks, tents and vehicles. Continuous autonomous operations require sensing of these terrain types and obstacles under all conditions of visibility, often including those of blowing snow. These conditions provide the impetus for the investigation and testing of sensing modalities that can withstand the Antarctic environment. Vandapel et al. deployed stereo cameras and laser rangers in the same polar region [1]. Preliminary conclusions indicate that stereo vision performed poorly on cloudy days because of lack of contrast. Blowing snow limited the laser sensors because snowflakes reflected the laser beam resulting in erroneous distance measurements. The field party had similar problems that limited the researchers' operation and exploration tasks because of impaired terrain perception [2].

B. The Sensor

Millimeter-wave radar has been used extensively for applications that require fine angular resolution with a limited antenna size. This investigation used a mechanically scanned millimeter-wave radar designed for obstacle avoidance and road navigation in heavy-dust conditions.

The sensor is a bistatic 77-GHz FMCW millimeter-wave radar. The wavelength is $\lambda = 4mm$. The beamwidth is 2° in elevation and 1° in azimuth. The bistatic-antenna pair scans horizontally across the angular range of 64°. Simultaneously in intervals of 1° in azimuth, switches sequentially select four stacked-beam positions covering a total elevation range of 8°. One scanning cycle—or radar frame—covers a 64° by 8° area of the scene. The control interface allows for acquisition of consecutive scans.

A stand with a vertical-tilt axis allows the sensor to be aimed at different elevation or depression angles. Figure 1 presents side and front views of the sensor on the stand. The circle in the upper left corner is the window for a video camera that provides visual images for later use in comparison of the radar images.

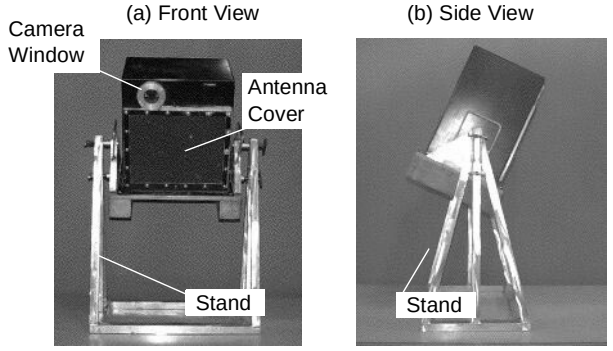

Fig. 1. Front (a) and side (b) views of the sensor. The pictures show the sensor at a depression angle adequate for terrain-surface sensing.

The sensor reports the amplitude of echoes at ranges between 1 and 64 m. The signal sampling provides amplitude measurements every 0.5 m. The sensor resolves range of targets separated by at least 1.5 m. Accuracy of the radar with appropiate processing is better than 0.25 m. Look-up compensation tables provide frequency stability for low-temperature operations.

II. Short-Range Radar-Sensing Issues

Radar sensing results in a range estimation calculated by the measurement of the time of flight for a transmitted radar signal from the radar antenna to the target and back. This process stems from wave propagation through the media and reflection on or scattering by the target back to the sensor. The range of interest for the mobile-robot application is from 1 to 100 m. The sensor used in this investigation limits the experiments to a maximum of 64 m.

A. Atmospheric Attenuation of Propagated Energy

Atmospheric and weather attenuation of millimeter-wave radar is significant for long-range sensing. The dry environment has a clear-air attenuation of the order of 0.2 to 0.4 dB/km, which has no effect on the range of interest. Flying snow and ice can cause an increase in attenuation. The size of snow and ice crystals is comparable to the millimeter wavelength; these forms of precipitation can attenuate or introduce noise into the range measurements. Several authors have investigated and modeled snow attenuation. Models of the snow crystals as hexagons allow the derivation of the absorption and scattering of millimeter waves in [3] and [4]. An experimental equation in [6] and [7] for calculation of the attenuation factor is

$$\kappa_{snow} = \frac{0.00349R^{1.6}}{\lambda^4} + \frac{0.00224R}{\lambda} \quad . \tag{1}$$

This equation for wavelength λ and rate of snow R (expressed in mm/h) gives values in the range of 0.2 to 1.0 dB/km. Similar to the case of clear-air attenuation, the equation predicts almost no effect of flying snow on millimeter-wave range estimation.

B. Antenna-Radiation Pattern and Pencil Beam

For robot perception, an accurate range map of the environment can be constructed through the scanning of a *pencil beam*. This is an antenna pattern with a single, narrow lobe. Millimeter-wave radar provides a pencil beam with a relatively small antenna aperture. The beamwidth is proportional to the wavelength and is inversely proportional to the antenna aperture. A constant antenna aperture shapes narrower beams at shorter wavelengths:

$$\theta = 1.02 \cdot \frac{\lambda}{D} \quad . \tag{2}$$

Equation (2) relates the beamwidth function of the wavelength and the antenna aperture. At 77 GHz, a wavelength of 4 mm, a 1° beam results from a 230-mm antenna aperture. A narrower beam produces more accurate terrain maps and obstacle detection. However, antenna size is limited by robot size and room availability. The lobe structure of the antenna radiation pattern outside the mainlobe consists of a number of sidelobes. Sidelobes result in a fraction of the radiated energy illuminating areas other than those in the desired mainlobe directions and in receipt of reflected energy from undesired directions. When the attenuation of sidelobes is poor, targets in directions other than those of the mainlobe appear in the radar signal. This particular radar provides a sidelobe attenuation of 15 dB below the mainlobe level.

C. Near/Far-Field Effect

Most radar applications sense targets in the antenna far-field region where the radiated power density varies inversely with the square of the distance and in which the antenna pattern remains constant for each angle. The beginning of the far-field region occurs at a distance R_{min} for which

$$R_{min} = \frac{D^2}{\lambda} \quad . \tag{3}$$

Equation (3) results in $R_{min} \approx 13.6m$ for the radar used in this study. Slow operations and actuator-related robot tasks require short-range sensing. Therefore, sensor targets often fall within the near-field region where the antenna pattern is range-dependent. Earlier work with millimeter-wave radar for robotic perception shows deformation of the beam in near-field conditions [8]. Additionally, bistatic radars such as the one used in this study introduce parallax distortions close to the pair of antennas. Near-field and parallax effects do not prevent sensing close to the radar, but suggest complex beam geometries and more difficulty in data interpretation.

D. Grazing Angle and Backscattering

Mobile-robot perception requires terrain perception for mapping and path planning. Sensors are usually directed at the front of the vehicle for obstacle avoidance as the vehicle moves forward. The sensor-location height is limited by the maximum mast height or other robot-design constraints. The scanning pencil beam intersects the ground at near-grazing angles with potential specular reflection. Specular reflection may impede range measurement for grazing angles. Figure 2 represents the pencil beam hitting the terrain surface at a grazing angle. The origin of the beam at the center of the bistatic antenna pair is $\underline{O}$. The proximal and distal borders of the footprint area illuminated by the divergence beam are $\underline{A}$ and $\underline{B}$, respectively. The height of the beam origin with respect to the terrain level is $\underline{h}$. The slant range from the beam origin to the intersection of the beam axis and the terrain is $\underline{R}$.

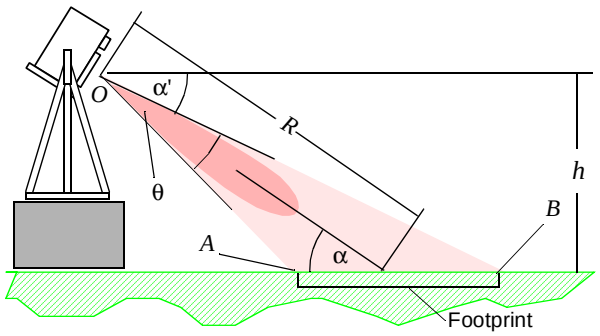

Fig. 2. Scheme of a pencil beam (beamwidth θ) sensing terrain at grazing angle α. The footprint is defined by the proximal border *(A)* and the distal border *(B)*. The sensor-depression angle is α'.

Scattering and specularity at grazing angles have been investigated extensively on sea, ground and snow surfaces. These investigations produced models that predict reflection based on the terrain characteristics and the wavelength. A snow-scattering study that appears in References [9] and [10] presents a model for snow-surface scattering and experimental data at 35, 95 and 135 GHz. The study concluded that dry-snow roughness has no effect on the scattering. At 35 GHz, moisture content and roughness affect scattering. The same research group examined 95-GHz scattering at near-grazing incidence for a variety of terrain surfaces, validating the Rayleigh criteria that defines scatter conditions [11]. If δh is the root-mean-square surface roughness, α is the grazing angle and λ is the wavelength, then a surface is not rough when

$$\delta h \sin\alpha \le \frac{\lambda}{8} \ . \qquad (4)$$

When the relation is satisfied, the surface scatters the beam—thus providing reliable perception. If the condition is not satisfied, it could mean that the reflection is specular with no return to the radar for range estimation. Figure 7 shows a blue-ice field, a common surface type for Antarctic-robot tasks. Although the ice is smooth, the wind carves shapes that should provide scatter.

E. Grazing Angle and Footprint Shape

Grazing angles stretch the pencil-beam footprint. This results in range-echo spread. Figure 2 illustrates the grazing angle and footprint. Figure 3 shows the corresponding echo spread. This scheme assumes that backscatter exists and that the footprint is within far-field conditions, which give the beam a conical shape. The footprint is the major axis of an ellipse with longitude $|AB|$ determined by a slant range to the surface R with grazing angle α and with beamwidth θ. For pencil beams the footprint length can be approximated as

$$|AB| = \frac{R \cdot \theta}{\sin\alpha} \ . \qquad (5)$$

The width of the echo spread in the radar signal S_{echo} is $|OB| - |OA|$, different from the footprint length on the surface. A theoretical value for S_{echo} results from

$$S_{echo} = \frac{h}{\sin\left(\alpha - \frac{\theta}{2}\right)} - \frac{h}{\sin\left(\alpha + \frac{\theta}{2}\right)} \ . \qquad (6)$$

The signal returned from sensing at grazing angles has the shape shown in Figure 3. The ratio between the amplitude of the echo and the noise level in the proximity of the echo provides a measure of the returned-energy strength.

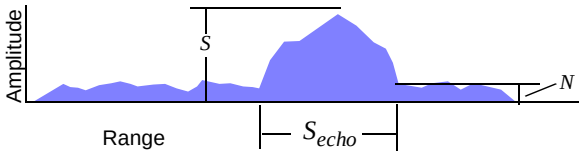

Fig. 3. Expected signal from grazing-angle perception. The echo spread S_{echo} is a function of the grazing angle, the beamwidth and the slant range from the sensor to the surface. The signal level is *S*. The noise level is *N*. The ratio *S/N* represents the strength of the echo.

A graph of the simulated footprint profile of a pencil beam (as represented in Figure 2) appears in Figure 4. This figure graphs the surface-echo spread calculated from Equation (6) and corresponds to S_{echo} as illustrated in Figure 3.

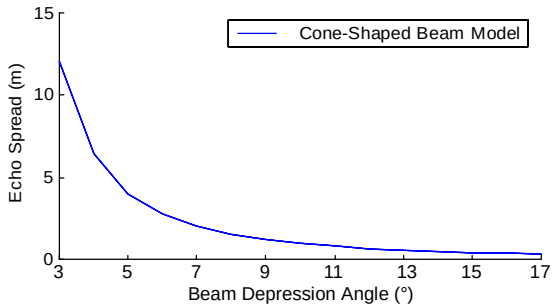

Fig. 4. Predicted footprint profile for a conical beam model over flat and level terrain (beamwidth 2°).

III. Sensing Under Conditions of Blowing Snow

Radar-data acquisition for this experiment occurred in two sessions: one with a clear-air atmosphere and the second under severe blowing-snow conditions. The clear-air-atmosphere session provided a reference for the inherent sensing noise in perfect visibility. The sensing comparison demonstrated the expected potential of radar to provide robust sensing in the harshest polar weather.

The radar was deployed in a horizontal area and was pointed in a fixed direction. The scene had a clear area of snow as well as a tent, a wooden box, a snowmobile and small objects scattered around the area (Figure 5).

The sensor acquired frames of the scene at a beam-depression angle of 7°. The beam-depression angle and a sensor height of 1.6 m result in a slant range of 13.1 m from the center of the footprint on the surface. Equation (5) indicates a footprint length of ~3.8 m.

Figure 6 shows a bidimensional intensity graph of the radar data for one beam across the horizontal scanning angular range. The horizontal axis represents the horizontal scanning angle. The vertical axis represents the slant range from the sensor. The dark gray areas represent the intensity of the obstacles echoes, light gray indicates absence of backscatter and black indicates saturation or the maximum value of received energy. It is possible to observe echoes of the obstacles in Figure 5, which are represented by dark areas in Figure 6.

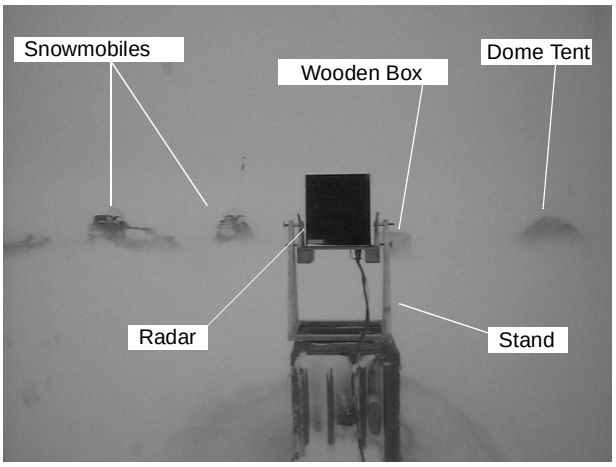

Fig. 5. View of the back of the radar as it points to the reference scene. This picture was taken under medium intensity of blowing snow. The targets become invisible when heavy blowing-snow conditions develop. The sensor acquired data under conditions of heavy blowing snow and under clear-air conditions.

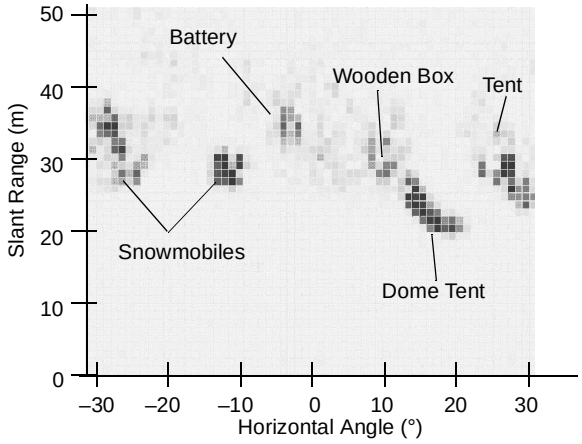

Fig. 6. A selected radar-data frame showing the intensity of the returned energy with respect to range and horizontal angle. The dark areas indicate the stronger echoes corresponding to obstacles. The graph is in polar coordinates and the objects appear distorted due to the projection in the rectangular grid.

Radar data from the selected beam position was divided in two sets of five frames for analysis. The first corresponded to the data acquired on the clear-air day. The second set contained data acquired under blowing-snow conditions. A visual inspection of all radar frames indicated that all the objects were present in each frame. One immediate conclusion is that—with this radar and within ranges of 40 m or less—all objects of interest appear in the frames, and obstacle detection is possible. The weather condition does not prevent the detection of the objects in the area of interest.

Some radar-data frames contained noise not related to the weather. The origin of the noise in those frames was thought to be inherent to the radar or other sources not related to the weather. Those frames were discarded as useless for statistical analysis. The noise (weather related) contained in the remaining frames of the two sets was measured. The analysis results in Table I compare noise values for both weather conditions.

TABLE I
STATISTICAL ANALYSIS OF NOISE INTRODUCED BY BLOWING SNOW

Weather Condition	Max. Average	Max. STD
Clear Air	409	45.75
Blowing Snow	422	50.75

The column Max. STD (maximum standard deviation) in Table I indicates the maximum variation in the values of the amplitudes for all five frames. In other words, the location with the energy value that changed the most in the five frames taken under blowing-snow conditions has a standard deviation approximately 10% greater than the location that had the most variation in clear-air conditions. As a reference, the Max. Average column indicates the maximum average of the energy values of the frame set. The table values and the frame observations indicate that blowing-snow slightly increases noise compared to clear-air conditions but does not prevent detection of common obstacles.

IV. BACKSCATTER FROM POLAR TERRAIN AT GRAZING ANGLES

The backscatter test examines the energy reflected back at different grazing angles on blue ice, soft (fresh) snow and hard (packed) snow. A flat and level area was selected on soft-snow, hard-snow and blue-ice fields. The sensor acquired data in three sessions under clear air, one session for each type of terrain. In each session, the sensor acquired data at seven beam-depression angles from 3° to 17° in increments of 2°. The beam-depression is equal to the grazing angle because the surfaces are flat and level.

Fig. 7. Blue-ice field, a common terrain type in Antarctica. It contains reliefs carved by the wind. The small holes or “ice cups” are approximately 10 cm in diameter and 5-cm deep with smooth contours. Even though the ice surface can appear specular, the ice cups provide relief for backscatter at low grazing angles.

Soft snow and hard snow are surface types found in environments other than polar ones. Blue-ice surfaces are unique to polar regions such as Antarctica. Blue-ice surface is solid ice, and it contains reliefs carved by the wind. The small holes or “ice cups” are approximately 10 cm in diameter and 5-cm deep with smooth contours. Even though the ice surface appears specular, the ice cups provide relief for backscatter at low-graz-

ing angles. Figure 7 shows a picture of the Patriot Hills blue-ice field.

The existence and strength of the backscatter echo is estimated from the plots, identifying the echo and its value over the noise in its proximity. Figure 8 presents raw radar data with the energy returned by the blue-ice surface. Each plot has seven signals superimposed that provide an estimation of the repeatability of the measurement. Each signal corresponds to one beam, and the difference indicates the inherent noise in radar measurements.

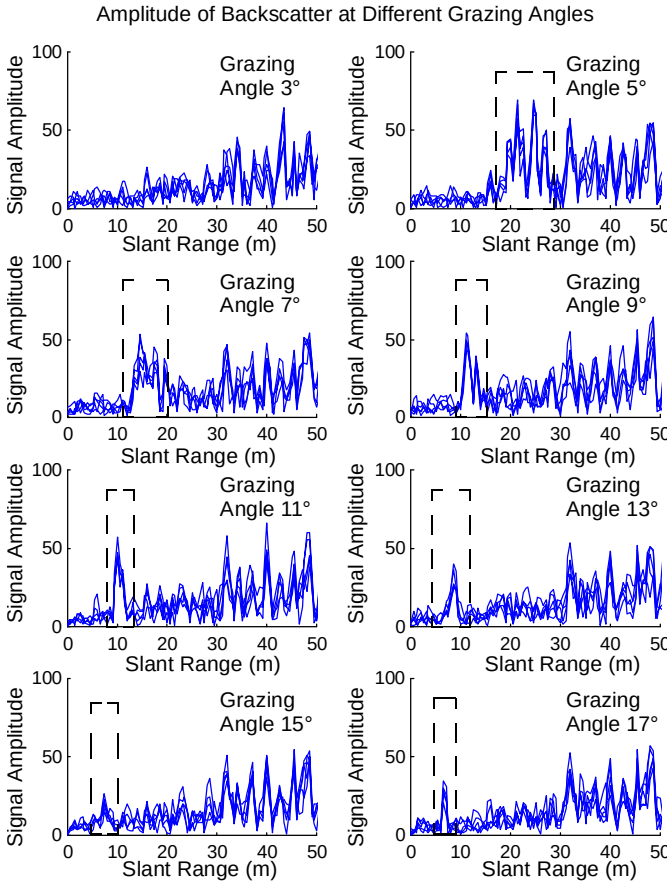

Fig. 8. Comparison of the backscattered-energy amplitude versus slant range for increasing beam-depression angles. The eight plots correspond to the beam-depression angles 3°–17° in steps of 2°. The outline of a vertical rectangle in each graph highlights the surface echo (except the first that does not show echo).

All graphs show that at slant ranges of 30 m and farther the signal contains a pattern that does not relate to the depression angle. This pattern is internal noise in the equipment, and it does not compromise echoes in shorter ranges or strong signals. However, this noise pattern can hide the echo for the lowest grazing angle. This experimental data indicates the existence of backscatter for grazing angles of 5° or more. Because of the internal sensor noise, the data does not provide evidence of *absence* of backscatter at grazing angles lower than 5°.

Similar plots from the sessions on soft snow and hard snow allow estimation of the signal-to-noise ratio, or signal strength for each type of terrain. Figure 9 presents the experimental echo strength for the backscatter at grazing. In all cases, there is no signal at a depression equal or less than 3°. The noise pattern in the radar can explain the absence of echo for low grazing.

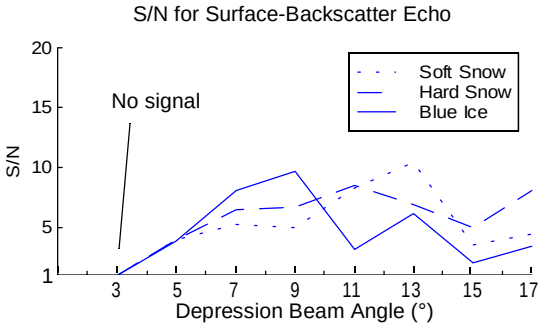

Fig. 9. Signal-to-noise ratio for the surface-backscatter echo versus grazing angle. Each plot represents the relative strength of the signal returned by the surface at each beam-depression angle.

The Rayleigh criteria applied to millimeter waves at 77 GHz appears in Figure 10. The graph indicates a height deviation of approximately 10 mm for a grazing angle of 3°. The height deviation for blue ice is of the order of 30 mm. Additionally, earlier work in [9] and [10] indicated that the grazing angle does not affect backscatter in dry snow, such as that found in Antarctica. This evidence confirms that the lack of echo at grazing angles of 3° is explained by noise in the radar that hides weak signals and is not the result of specular reflections.

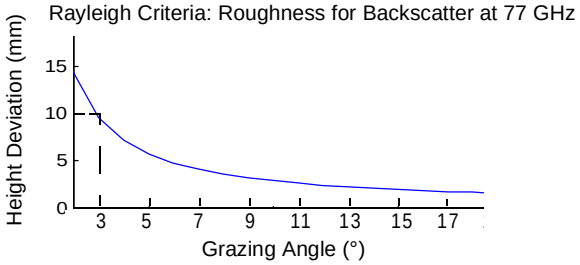

Fig. 10. Rayleigh criteria: height deviation required for backscatter of millimeter waves at 77 GHz (4 mm). The dashed line indicates the height deviation required for backscatter at grazing angle of 3°.

The experimental data shows that the relief of soft and hard snow, as well as the relief of blue ice scatter millimeter waves at low grazing angles. The scatter at grazing enables look-forward robot sensing based in millimeter-wave radar.

V. Short-Range Sensing Footprint Analysis

This section compares the theoretical footprint size and the experimental results based on the same data of the previous experiment: backscatter on polar terrain at grazing. Figure 11 plots the experimental values for the slant range based on the proximal and distal sides of the footprint as well as the width of the footprint echo, which corresponds to S_{echo}.

The cone-shaped beam model (shown in Figure 4) fails to predict the width of the footprint echo, especially at short ranges. Possible causes include the following: a different beam model due to incorrect beamwidth, near-field effect, and nonlevel or nonflat terrain. However, instances of nonflat terrain or incorrect beamwidth will result in errors at farther ranges. The errors

in shorter slant ranges are thought to be related to near-field effect.

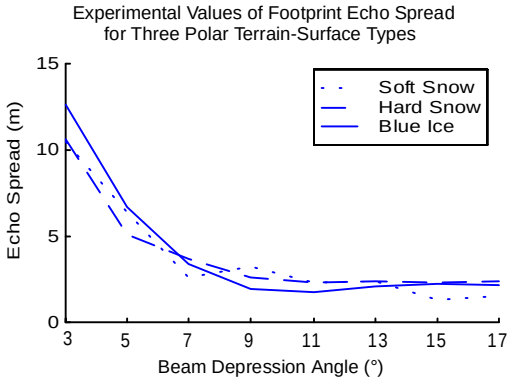

Fig. 11. Experimental footprint profiles for three surface types: blue ice, hard snow and soft snow. The echo spread is constant for depression angles greater than 9°.

An alternate beam model based on the results presented in [8] was implemented to simulate the near-field effect. This model represents the beam as a cylinder of the antenna diameter that extends from the antenna face to the far/near field distance. From there, it follows the same shape as the cone-shape beam model. Figure 12 presents a scheme of the cylinder-cone model (a) and the simulated footprint-echo spread (b). The simulated footprint results in a constant width for the footprint echo similar to the experimental data.

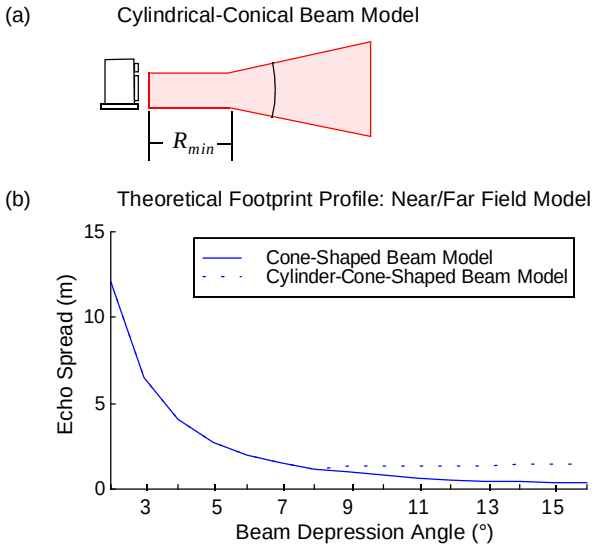

Fig. 12. Beam profile with cylinder representation of near field. The length of the cylinder is calculated in Equation (3), $R_{min} \approx 13.6m$.

The alternate model performed better than the common cone-shaped beam model at predicting the surface-echo spread at short ranges. The consideration of near-field effect improved the interpretation of short range data. This result suggests that beam models that consider near-field effect are necessary for robotic sensing of close objects based on millimeter-wave radar.

VI. Conclusion

This paper presents the analysis and results of experiments conducted with a short-range millimeter-wave radar on polar terrain. The analysis of the field data shows that millimeter-wave radar functions adequately in compromised visibility conditions. Presence of blowing snow slightly increases scene noise but does not prevent sensing of obstacles. Ice and snow surfaces provide enough reflection for detection and backscatter from the polar surfaces is obtained at grazing angles as low as 5°. There is evidence that scatter at lower angles exists but is hidden by the sensor noise. Differences between the expected footprint and the experimental values are explained with near-field effect. Consideration of near-field effect improves radar data interpretation and prediction. Radar sensing exhibits better reliability than laser and stereo under some conditions, thus making this sensing modality a good candidate for robotic perception.

Acknowledgments

The authors thank the Robotic Antarctic Meteorite Search Program for the support and funding of this research. This program was funded by the Telerobotics Program NAG 5-7707 of NASA's Office of Space Science, Advanced Technology and Mission Studies Division. The authors value the logistical support provided at Patriot Hills, Antarctica, by the Chilean Air Force and Chilean Antarctic Institute.

References

[1] N. Vandapel, S. Moorehead, W. Whittaker, R. Chatila and R. Murrieta-Cid, "Preliminary Results on the Use of Stereo, Color Cameras and Laser Sensors in Antarctica," *Proceedings of the International Symposium on Experimental Robotics*, 1999.

[2] Unpublished field-team reports on environmental conditions during January and November of 1998 in Patriot Hills, Antarctica, Robotic Antarctic Meteorite Search Program.

[3] P. Chylek, J. Zhan and R. Pinnich, "Absorption and Scattering of Microwaves by Falling Snow," *International Journal of Infrared and Millimeter Waves*, vol. 14, no. 11, 1993.

[4] A. Osharin, "Millimeter-Wave Scattering by Dry Snow Crystals," *Radiophysics and Quantum Electronics*, vol. 37, no. 11, 1994.

[5] E. Vinyaikin, M. Zinicheva and A. Naumov, "Attenuation and Phase Variation of Millimeter and Centimeter Radio Waves in a Medium Consisting of Dry and Wet Dust Particles," *Radiophysics and Quantum Electronics*, vol. 37, no. 11, 1994.

[6] T. Frey, "The Effects of the Atmosphere and Weather on the Performance of a mm-Wave Communication Link," *Applied Microwave & Wireless Magazine*, vol. 11, no. 2, February 1999.

[7] N. Currie and C. Brown, *Principles and Applications of Millimeter-Wave Radar* (Artech House Inc., Boston, 1987).

[8] M. Lange and J. Detlefsen, "94 GHz Three-Dimensional Imaging Radar Sensor for Autonomous Vehicles," *IEEE Transactions on Microwave Theory and Techniques* vol. 39, no. 5, 1991.

[9] Y. Kuga, F. Ulaby, T. Haddock and R. Deroo, "Millimeter-wave radar scattering from snow: 1. Radiative transfer model," *Radio Science*, vol. 26, no. 2, 1991.

[10] F. Ulaby, T. Haddock, R. Austin and Y. Kuga, "Millimeter-wave radar scattering from snow: 2. Comparison of theory with experimental observations," *Radio Science*, vol. 26, no. 2, 1991.

[11] F. Ulaby, A. Nashashibi, A. El-Rouby, E. Li, R. De Roo, K. Sarabandi, R. Wellman and H. Wallace, "95-GHz Scattering by Terrain at Near-Grazing Incidence," *IEEE Transactions on Antennas and Propagation*, vol. 46, no. 1, January 1998.